IEEE Access
Multidisciplinary | Rapid Review | Open Access Journal

Received 11 June 2023, accepted 31 July 2023, date of publication 7 August 2023, date of current version 16 August 2023.

Digital Object Identifier 10.1109/ACCESS.2023.3303347

RESEARCH ARTICLE

Lossless Compression and Linear Recovery of a System Matrix Based on a Polar Adaptive Pixel

SHUYI CHEN, MIN ZHAO, MIN YAO, RUIPENG GUO, AND MING WANG

College of Automation Engineering, Nanjing University of Aeronautics and Astronautics, Nanjing 211106, China
Nondestructive Detection and Monitoring Technology for High-Speed Transportation Facilities, Key Laboratory of Ministry of Industry and Information Technology, Nanjing 211106, China

Corresponding author: Shuyi Chen (chenshuy828@163.com)

This work was supported in part by the Natural Science Foundation of China under Grant 62071229, and in part by the Postgraduate Research and Practice Innovation Program of Nanjing University of Aeronautics and Astronautics (NUAA) under Grant xcxjh20220302.

ABSTRACT The nondestructive characteristics of γ-photon imaging technology make it attractive potential in the industry. However, in industrial detection with a large detection range and high resolution, iteration method, the image reconstruction algorithm which is most widely used, faces the challenge of an overly large system matrix, and the current compression algorithms using the geometric symmetry of the positron emission tomography (PET) system have problems of complex pixel division and recovery mode. Therefore, this study proposes a lossless compression and linear recovery algorithm of the system matrix based on a polar adaptive pixel (LCLR-PAP). Based on the structure of the detection ring and rotation of the circle, the detection field of view (FOV) is designed as a cylinder and the circular slice is divided into several sectors. The pixels are adaptively divided within the sector to realize the lossless compression of the system matrix from the structure, and based on which the angle change of pixels can be converted to matrix transformation to achieve linear recovery. A partial pixel partition is optimized to compensate for the unevenness of the pixel size in the center of the adaptive image. Experiments show that the LCLR-PAP algorithm can provide an efficient solution to the large-scale system matrix compression recovery problem, that is, through a simple and convenient adaptive pixel division with matrix sparsity and axial symmetry, the system matrix can be compressed to less than 100,000th of the original, and realize the lossless compression and fast linear recovery.

INDEX TERMS Adaptive pixel, compression algorithm, gamma photon imaging, system matrix.

I. INTRODUCTION

Gamma photon tomography uses paired gamma photons produced by positron annihilation to observe the internal state of an object. Gamma photons produced by positron annihilation have the characteristics of strong penetration and anti-interference ability [1], can easily pass through the workpiece to be tested, and can overcome extremely harsh environments, such as high temperature, high pressure, and high speed. The positron annihilation technology be utilized as a good means of industrial nondestructive testing because of these characteristics [2]. The positron image reconstruction algorithms are mainly divided into analytical methods and iterative methods from the theoretical standpoint. The analytical method is based on the Fourier central slice theorem, and the image reconstruction is achieved by back-projection, the most common of which is the filter back-projection (FBP). The analytical method has the advantages of fast and simple reconstruction, but some noise or interference occurs during data acquisition, so the reconstructed image quality is low [3]. Iterative methods can solve the defects of analytical methods, which are divided into algebraic iteration and statistical iteration, among which the Maximum Likelihood Expectation Maximization [4] (MLEM) and Ordered Subset Expectation Maximized [5] (OSEM) are the most widely used. The system matrix is an important parameter in an iterative method [6].

The system matrix stores the probability of coincidence events being detected by each pair of detectors, which is

The associate editor coordinating the review of this manuscript and approving it for publication was Zhan-Li Sun.

the basis of accurate ortho-projection and back-projection operations in the iterative reconstruction algorithm, and is directly related to the quality of the output image [7]. With the continuous maturity of γ-photon tomography technology, it is possible to apply γ-photon tomography technology in industrial nondestructive testing. For example, in the internal diagnosis of aircraft landing gear hydraulic system [8], high-resolution γ-photon tomography technology can help to detect cracks; in terms of flow field imaging [9], the high-resolution γ-photon tomography technology can observe the situation in the closed cavity, which is conducive to the analysis of flow field state; in the detection of the flow field of the engine combustion chamber, the large-diameter γ-photon tomography technology helps to realize the in-situ detection without disassembling the object to be measured. However, industrial nondestructive testing requires a large detection range and high resolution, increasing the amount of system matrix data in image reconstruction, which limits the further development of this technology in industrial nondestructive testing. Taking the small positron imaging device as an example, when the number of coincidence events is $156 \times 156 \times 52 \times 52$, if the three-dimensional image with the resolution of $400 \times 400 \times 52$ is taken as the research object, the number of elements in the system matrix is 5.47×10^{14}. If saved as a single-precision floating-point number, it would take up about 1.95 PB of space. Even if the study is done with two-dimensional images, the size of the system matrix will reach 14.51GB. The huge system matrix may face the problem that it cannot be loaded into the computer memory at one time, and at the same time, as the system matrix increases, the generation of the system matrix will take a substantial amount of time and occupy a large storage space in the case of high-resolution image reconstruction, and the time of image reconstruction will also greatly increase. In theory, the Monte Carlo simulation method can obtain the best system matrix generation accuracy [10], but the generation time sharply increases in the industry. Therefore, a high-precision system matrix is difficult to quickly generate and apply to engineering practice without system matrix compression. In this paper, we will provide a system matrix compression method that can greatly compress the computational data and recover them loss-less, to solve the problems of large system matrix and large computation, which makes the application of γ-photon technology in large space and high-resolution industrial nondestructive testing possible.

In the research on the compression storage of the system matrix, the methods used to solve the space occupied by the system matrix mainly include real-time calculation, system matrix decomposition, and compression using the symmetry of the detector structure. The method of real-time calculation is used to calculate the required system matrix elements at any time in the reconstruction process. The system matrix is calculated in real-time during each forward and backward projection. In 2008, Kadrams et al. [11] proposed a rotating and oblique projection method, but the resulting forward and backward projections may not match. In 2012, Zhang et al. [12] realized real-time computing of the system response matrix based on the optimized Siddon algorithm for list-mode reconstruction. However, the real-time calculation of the system matrix required a large number of computing resources, and recalculation was required every time during the iteration process, which seriously affected the reconstruction speed [13]. Given that the matrix decomposition can produce a sparse matrix, the system matrix can be calculated and stored in advance through the system matrix decomposition method. The implementation of forward and backward projection only requires sparse matrix and vector multiplication. In 1998, Qi et al. [14] used the matrix decomposition method to decompose the system matrix into a geometric projection matrix, a sinogram fuzzy matrix, and an image fuzzy matrix. However, this method would result in a large geometric projection matrix at high-resolution reconstruction. In 2011, Zhou et al. [15] proposed a new method that uses a simpler geometric projection matrix to further reduce the nonzero values. The method of decomposing the system matrix can greatly reduce the size of the stored system matrix, but it also introduces oversimplification, resulting in a relatively large fuzzy effect on the quality of the reconstructed image.

Another compression idea is to use some characteristics of the system matrix itself and reduce them based on the symmetry of the detector ring structure. The idea of using the geometric symmetry of the PET system to compress the matrix is the most direct and has been proven to be effective [16].In 2003, Rafecas et al. [17] used the inherent symmetry in the MADPET-II matrix to find four identical system matrix weight values by dividing the field of view (FOV) into four equal parts and compressing the system matrix fourfold. In 2004, Rannou and Chatziioannou [18] used the rotation symmetry between the detector rings in a Monte Carlo simulation and compressed the system matrix to one-eighth of the original by using four cross-axes and one axial symmetry. In 2011, Scheins et al. [19] segmented several triangular regions according to the intrinsic symmetry of the PET system and tangentially subdivided the triangular slices to obtain specific pixel sizes for achieving multi-fold compression of the system matrix. The compression rate was improved compared to the previous ones, but the pixel shapes were diverse, the division was complicated, and the FOV edges were not smooth and polygonal. In 2013, Yu et al. [20] adopted rotating symmetric polygon pixels, established the geometric definition and index rules of the polygon pixels and compressed the system matrix by eight times, but there are still problems such as complex pixel division and uneven shape. Meanwhile, the system matrix recovery mode of the index is also complicated. In 2015, Ahmed et al. [21] made use of the diagonal characteristics of the square to compress the system matrix eightfold. In 2017, Sun et al. [22] compressed the system matrix multiple times according to the detector structure and square symmetry, but its pixels did

not fully coincide in rotation, resulting in recovery errors. In 2021, Deng et al. [10] calculated only 1/8 of the system matrix according to the intra-ring symmetry of the rectangular detector, obtained the SM of other parts through geometric transformation and compressed the calculation of the system matrix of slice direction eightfold, but it did not apply to the polygon detector.

The large-scale compression using geometric symmetry at present has some problems, such as complicated pixel division, pixel irregularity, unsmooth edge of the FOV, or complicated recovery mode. This work proposes a lossless compression and linear recovery algorithm of the system matrix based on the polar adaptive pixel to achieve the compression of the system matrix and address the problems in the compression process. Lossless compression of the system matrix is realized by circular detection FOV and rotation of polar coordinates in combination with adaptive pixel division. The equivalent relationship between the rotation of the response line in the polar coordinates and the translation of the system matrix is obtained on the basis of this model to realize the rapid recovery of the system matrix. The algorithm is also optimized to solve the problem of uneven center in adaptive pixel partition. The characteristics of the algorithm are as follows:

1. The smooth boundary of the polar coordinate circular FOV ensures the lossless and efficient algorithm from the structure and provides the prerequisite for the rotation of pixels; fully utilizes the structural characteristics of the detector and the rotation of the circle to achieve the rotational overlap of pixels; maximizes the use of the characteristics of the positive polygon of the detector to achieve the multi-fold compression of the system matrix;

2. Adaptive sector ring (sector) pixel shape is simple, easy to divide, and convenient to store, which can realize lossless compression of the system matrix. From the storage and calculation point of view, the image consists of only the first layer of the sector, and the sector ring in the other layers, with no other graphics, and the graphics in each layer are consistent, and each layer only needs to be calculated once; when storing the graphics, only the number of layers divided, and the number of pixel divisions in each layer needs to be stored, and the complete pixel distribution can be obtained. At the same time, the adaptive pixels not only ensure the quality requirements of the reconstructed image but also the pixels at the boundary of the sector are completely divided, thus realizing the lossless compression of the system matrix;

3. Due to the polar adaptive pixel, the system matrix can achieve linear and fast recovery. Based on the Line of Response (LOR) rotation invariance, only a subset of the system matrix needs to be stored, and the values of the system matrix that are not stored can be obtained from the stored subset by a linear transformation of the matrix, which avoids the use of auxiliary matrix recovery, reduces the workload, shortens the recovery time, and avoids errors.

II. SYSTEM MATRIX COMPRESSION AND RECOVERY BASED ON A POLAR ADAPTIVE PIXEL

A. STATISTICAL ITERATIVE ALGORITHM

The iterative method is the most widely used reconstruction algorithm, represented by MLEM and OSEM. The MLEM [23] algorithm uses maximum likelihood estimation to reconstruct the image. Pixels will continuously decay and release positrons. The PET detector detects that the annihilation process of the positrons conforms to the Poisson distribution and is independent and identically distributed. The iterative formula of the MLEM algorithm can be obtained according to the principle of maximum likelihood:

$$x_j^{k+1} = \frac{x_j^k}{\sum_{i=1}^{I} a_{ij}} \sum_{i=1}^{I} a_{ij} \frac{y_i}{\sum_{j=1}^{J} a_{ij} x_j^k}, \tag{1}$$

where x_j^{k+1} is the pixel value after the $k+1$ iteration of the reconstructed positron image pixel j, x_j^k is the pixel value after the k iteration of the pixel j, y_i represents the ith sinogram component (the detection result of the ith LOR), and a_{ij} represents the ith row and jth column element values of the system matrix.

In the MLEM reconstruction algorithm, every iteration needs to traverse each system matrix element and image pixel, and the convergence speed of the algorithm is slow [4]. On this basis, the OSEM reconstruction algorithm is proposed [24]. OSEM reconstruction algorithm is the most commonly used algorithm in the current iteration algorithms, and its subsets the system matrix and sinusoidal graph based on the MLEM algorithm. Moreover, the OSEM algorithm can divide the huge system matrix into N subsets in the way of ordered subsets to reconstruct the image, which effectively reduces the number of iterations [25]. A subset iteration of the OSEM algorithm is equivalent to a complete iteration of the MLEM algorithm. After completing one iteration of all subsets, the image reconstruction effect is equivalent to the effect of N iterations of the MLEM algorithm. However, the calculation amount is only equivalent to that of one iteration of the MLEM algorithm.

The selection of subsets in the OSEM reconstruction algorithm follows the following criteria:

(1) Each subset contains the largest amount of reconstructed image information and as much projection information as possible, and the information in the subset is uniform.

(2) The size of each subset is equal (i.e., each subset contains the same number of projection angles).

B. CONSTRUCTION OF SYSTEM MATRIX

The system matrix describes the response process of the detector to the detected space. This matrix is composed of the mapping relationship between the detector crystal and the pixels of the area to be reconstructed, and it connects all the pixels of the reconstructed image with the coincidence events in the detected space. The system matrix is a 2D matrix, and 1D of the system matrix represents the pixels in the imaging

field detected by the positron emission tomography system. The higher the density of pixels, the higher the resolution of the reconstructed image, and the wider the distribution range of pixels, the larger the detection field of the imaging system. The density and range of pixels are related to the physical structure of the imaging system. The other dimension of the system matrix represents the coincidence events collected by the detector of the imaging system. The coincidence events are determined by the crystal lines on the ring detector.

The system matrix establishes the physical model between the detector and the measured object. When the image is reconstructed by an iterative method, the system matrix establishes the relationship between the response line and the pixel, which is the key to the iterative method of image reconstruction. The formula is expressed as follows:

$$Y = AX, \tag{2}$$

where $Y = [y_1, y_2, \cdots, y_i, \cdots, y_I]^T$ is the vectorized sinogram of the data collected by the detector after recombination (I is the number of LOR), $X = \left[x_1, x_2, \cdots, x_j, \cdots, x_J\right]^T$ is the vectorized image pixel (J is the number of pixels), and A represents the complete system matrix. In the iterative image reconstruction algorithm, the element value of each system matrix a_{ij} represents the probability that the γ-photon pair emitted in the space covered by the jth pixel is detected by the ith crystal pair of the peripheral detector ring:

$$A = \left\{a_{ij}\right\}. \tag{3}$$

The element value of the system matrix is the probability of each pixel annihilation producing γ-photon pairs captured by the detector crystal. The accuracy of the system matrix elements will have a direct effect on the quality of the reconstructed image. Accordingly, the accurate system matrix can improve the quality of the image reconstruction, indicating that it is vital in the iterative reconstruction process of the γ-photon imaging system. Furthermore, the determination of the system matrix needs to consider the geometric structure of the detector system and the resolution of the image to be reconstructed. In practice, the system matrix only needs to calculate once and can be reused for the same resolution model. In industrial applications with a large detection range and a high resolution, the generation of the system matrix takes a substantial amount of time and occupies huge storage space and the time of image reconstruction increases. Therefore, an efficient and convenient system matrix compression method is needed to make this mechanism applicable to engineering practice.

C. POLAR ADAPTIVE PIXEL AND SYSTEM MATRIX COMPRESSION

In the study of the compressed storage of the system matrix, the idea of using the geometric symmetry of the PET system to compress the matrix is the most direct and has been proven to be effective. Given that the positron PET detection rings are mostly circular, multiple detector rings form a cylinder.

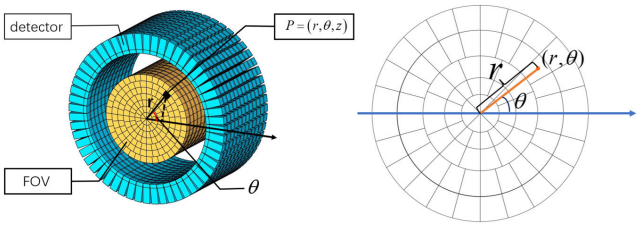

FIGURE 1. Schematic of the cylindrical FOV.

Accordingly, so the optimal imaging region of the γ-photon detection equipment is also a cylinder. In this work, the general quadrilateral FOV is improved to a cylindrical FOV, and the section of the cylindrical FOV is circular. When the detector has a normal N-edge shape, the compression ratio is N. The FOV can be divided into N sectors by drawing P rays from the center of the circular FOV, and the angle between adjacent rays is the top angle of each sector (θ=2π/N). Each sector has the same shape and equal area. The polar coordinate system is introduced on the basis of the circular FOV to discretize the FOV into a polar coordinate array (Fig. 1). This study uses the structural characteristics of the detector and the rotation of the circle, through the rotation to achieve complete coincidence and the detector's regular polygon characteristics to compress the system matrix. During the partition of pixels in the sector, the compressed system matrix can be recovered losslessly. Thus, the partition of pixels needs to consider the edge, pixel size, reconstruction accuracy, etc.

Therefore, this study proposes a system matrix partition method based on the polar adaptive pixel to compress the system matrix. The selection of the system matrix affects the quality of the reconstruction, and the division of pixels in the system matrix should ensure the accuracy of the reconstructed image. Since lossless compression is required, it is necessary to ensure that the pixel area differences are small and that the boundary pixels of the sector are completely divided. Therefore, the following principles of adaptive adjustment of pixels are used to divide the pixels:

(1) The sector ring height of the pixels and the sector height of the first layer is determined according to the pixel edge length corresponding to the resolution required for reconstruction, which guarantees that the height meets the requirements for the accuracy of the reconstructed image while not being larger than the spatial resolution of pet, as shown in the following equation:

$$h = \frac{R}{N} \leq a, \tag{4}$$

$$h \leq q, \tag{5}$$

where a is the pixel side length corresponding to the resolution, h is the sector ring height and the first sector height, R is the radius of FOV, q is the spatial resolution of PET, and N is the minimum positive integer that makes the inequality tenable.

The sector area of the first layer is shown as follows:

$$S_1 = \frac{\theta}{2} h^2, \tag{6}$$

where θ is the degree of the sector top angle.

The area of the sector ring after the height of each layer is determined, as shown in the following equation:

$$S_m = \frac{\theta}{2} \left[(2m-1)\, h^2 \right], \tag{7}$$

where m is the number of the sector ring layer. In this case, if the internal area of each sector ring (sector) is divided into $k_1, k_2, \cdots, k_N$ small sector rings (sector), then its area is denoted as S_{mk}.

(2) The area of a pixel should not be greater than the area of a pixel in the Cartesian coordinates equal to its height to maintain the necessary image resolution [26], which should meet the following formula:

$$S_{mk} \leq a^2, \tag{8}$$

where S_{mk} is the pixel area of the small sector ring (sector) on the mth layer. Then $k_1, k_2, \cdots, k_N$ should meet the following requirements:

$$\begin{cases} k_m \geq \frac{\theta}{2a^2} h^2 & \mathrm{m} = 1 \\ k_m \geq \frac{\theta}{2a^2} \left[(2m-1) h^2 \right] & \mathrm{m} \neq 1 \end{cases}. \tag{9}$$

(3) The pixel located at the sector boundary overlaps with the sector boundary. The coincidence of the boundary can ensure the integrity of the boundary. Accordingly, the boundary can be directly rotated to restore or reconstruct iteration, simplify the whole calculation process, and avoid the error brought by the recovery process.

(4) The area difference between the pixels should be small, and the polar pixel should be "square" as much as possible. If the sector height is fixed, then the arc length of the small sector should be equal, which echoes the square pixel in the Cartesian coordinate system. The small pixel area difference is conducive to reducing the image quality loss caused by pixel nonuniformity. Subsequent conversion between the adaptive and the Cartesian pixels can also keep the image distortion at a low level.

(5) If the above-mentioned requirements are met, the number of pixels and the shape number are kept to a minimum, making it easy to store and calculate. Only two shapes of pixels exist in the PAP algorithm: sector ring and sector, and the size of the sector ring (sector) in each layer is the same, which conforms to the principle of the least number of shapes. Theoretically, the higher the image resolution is, the more details the reconstructed image contains. However, the higher the image resolution is, the worse the image. This condition is also limited by the spatial resolution of the PET system. Increasing the number of pixels can improve the resolution, but the best imaging quality can be obtained when the pixel size reaches the spatial resolution of the PET system. Further improving the imaging resolution is no longer necessary. Therefore, the minimum number of pixels is enough if the resolution is satisfied.

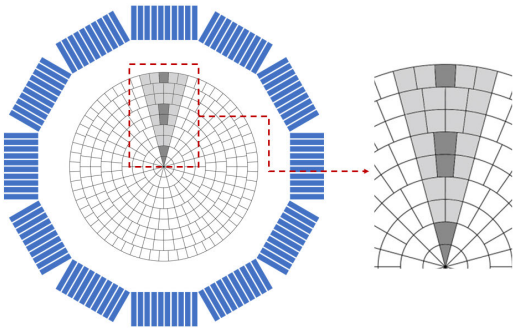

FIGURE 2. Adaptive pixel segmentation.

The polar adaptive pixel algorithm is proposed based on the circular polar coordinate FOV. If the FOV is divided into 12 parts according to the detector arrangement, the pixel partition is shown in Fig. 2, and each part is exactly equal and the internal pixel distribution is completely the same, which can be obtained by rotating the center of the circle, to realize the rotational symmetric compression of the system matrix.

The use of polar adaptive pixel division can also reduce the number of graphics and simplify the calculation process. From the perspective of the number of graphics, the image only consists of the sector in the first layer and the sector ring in the other layers, and there are no other graphics, and the graphics in each layer are consistent. From the perspective of adaptive pixel calculation and storage, since the graphics in each layer are consistent, each layer only needs to calculate one graphic; the radius of the pixels in each layer is determined, so the pixels only need to be transformed in angle; the angle transformation in each layer is consistent, and when storing the graphics, only need to store the number of divided layers and the number of pixels of each layer to obtain the complete pixel distribution. From the perspective of system matrix calculation, due to the rotational coincidence of each sector, after determining the number of sector segments, only the system matrix of pixels contained by one sector needs to be calculated to obtain a complete system matrix. Therefore, if the FOV is divided into N sectors, the calculation time of the system matrix will be compressed by N times. From the perspective of system matrix compression, only the system matrix of pixels in one sector ring needs to be calculated to obtain the system matrix of the other parts, and if the FOV is divided into N sectors, the system matrix will be compressed N times.

D. LINEAR RECOVERY OF THE COMPRESSED SYSTEM MATRIX

During the adaptive pixel partitioning, the area of the pixels in the middle circle of the image is often much smaller than that of the peripheral pixels, resulting in a difference in the pixel size. In the model reconstruction without LOR information at the center, the image reconstruction will not

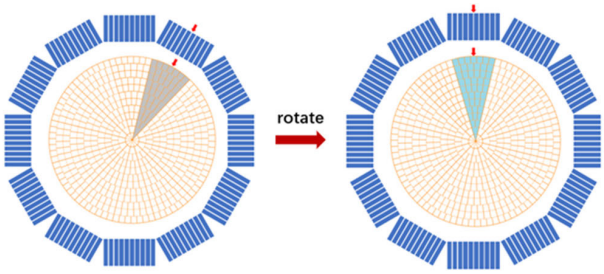

FIGURE 3. Schematic of adaptive pixel rotation.

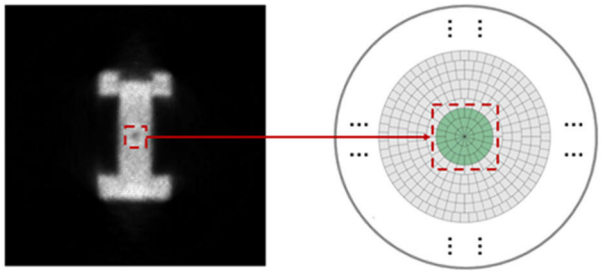

FIGURE 4. Artifacts in the central position of the image and their formation reasons.

have a quality impact, but if there is image information at the center, as in Figure 4, the non-uniformity of the pixel size will cause a black shadow, resulting in image quality loss. Therefore, this problem in pixel division should be considered and optimized.

The pixels designed in the central position are not divided according to the sector ring, but the whole circle (first layer) or the whole ring. The area division is based on the pixel size of the Cartesian coordinates, which retains the complete system matrix, and this part does not participate in pixel rotation.

If the pixel is divided in the compressed sector, when the pixel size of a layer is less than 80% of the square pixel with the same height, then the layer is divided by a complete circle (ring), as shown in the following formula:

$$S_{mk} = \begin{cases} \frac{\theta}{2k_m} h^2 \le 0.8a^2 & \mathrm{m} = 1 \\ \frac{\theta}{2k_m} \left[(2m-1)\, h^2 \right] \le 0.8a^2 & \mathrm{m} \ne 1 \end{cases}, \tag{10}$$

where m is the number of the sector ring layer, and the maximum $m_{\max}$ of m is taken. When the number of layers is $1, 2 \cdots m_{\max}$, the complete circle (ring) is divided into pixels.

The value of the sector segment number k_1 in the first layer is shown as follows:

$$k_1 = round(\pi h^2 / a^2), \tag{11}$$

where h is the height of the sector ring and the height of the first sector, and a is the pixel side length corresponding to the Cartesian coordinate system.

The area of the complete ring is as follows:

$$S_m = \pi \left[(2m-1)\, h^2 \right], \tag{12}$$

where m is the number of ring layers.

The other rings are divided into $k_2, \cdots, k_m, \cdots, k_{m_{\max}}$ small sector rings with an equal area. Then, the value of km is:

$$k_m = round(S_m / a^2). \tag{13}$$

E. LINEAR RECOVERY OF THE COMPRESSED SYSTEM MATRIX

In the study of system matrix compression based on rotationally symmetric polygons [20], YU used the polygonal property of FOV to achieve compression. The system matrix must be obtained through pixel indexing during the recovery process. A certain time loss is experienced in the indexing process, and some labeling principles and indexing rules must be formulated. However, in the case of rotational symmetry, certain structural relations must exist between different parts of the system matrix.

If the PET detector is divided into twelve equal parts according to its arrangement, then the twelve sectors are numbered as 1, 2, …, and 12. According to the rotational symmetry, only the system matrix corresponding to one equal part needs to be retained. Each part only accounts for one-twelfth of the number of elements of the whole system matrix. The other parts can be obtained by rotating the pixel index by 30 °, 60 °, …, 330 °, and the pixel rotation and its corresponding detector also rotate at the same angle. The corresponding system matrices and their direct values are the same. Only the translation of the matrix is required.

The system matrix of the other sector regions can be recovered by using the rotation symmetry of one sector region. When two pixels i and i_0 at different positions can be obtained by rotation, and the rotation angle of the two segments is φ, the following relationship is satisfied:

$$\varphi = m\theta, \tag{14}$$

where m is the sector number difference where the pixel is located, and θ is the top angle of the sector.

The distance between LOR_j and LOR_{j_0} to the pole is the same, and the vertical angle satisfies the following relationship:

$$\alpha_0 = \begin{cases} \alpha - \varphi & \alpha - m\theta \ge 0 \\ \alpha - \varphi + \pi & \alpha - m\theta < 0 \end{cases}. \tag{15}$$

Take Fig. 5 as an example, the relationship between pixels i and i_0 is: $\varphi = 120°$ and $\alpha_0 = \alpha - 30°$. The overlap area of pixel i and LOR_j is rotationally symmetric with that of pixel i_0 and LOR_{j_0}.Thus, the corresponding system matrix of pixel i and LOR_j has the same value as that of pixel i_0 and LOR_{j_0}, that is, $a_{i,j} = a_{i_0,j_0}$.

In Fig. 6, the orange LOR cluster and orange pixels were moved to the position of the green LOR cluster and green pixel by rotating the detector space 30 ° counterclockwise. The mapping relationship between the orange LOR cluster and the orange pixel is the same as that between the green LOR cluster and the green pixel due to the synchronous rotation of the detector and FOV in the whole process. In this

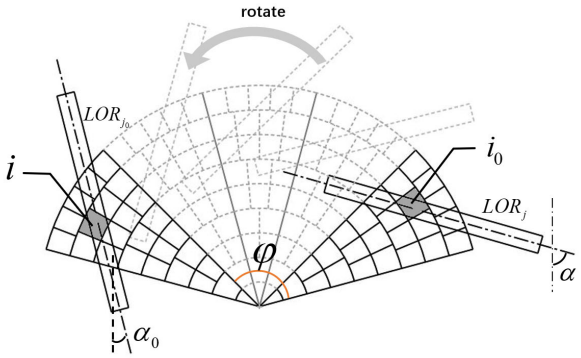

FIGURE 5. Schematic of the pixel rotation.

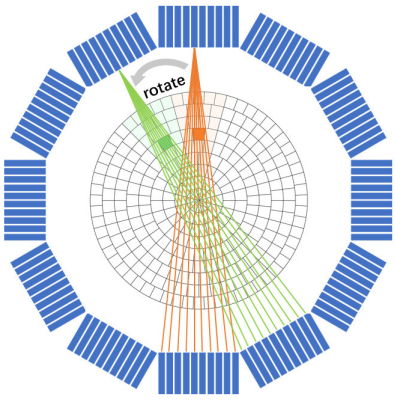

FIGURE 6. Schematic of the detector rotation.

way, only part of the system matrix elements formed by the corresponding relationship between the LOR and the image pixels can be stored, and the other system matrix elements can be calculated by rotation during the reconstruction.

When constructing the system matrix, we divide it according to angles. The n pairs of the crystals correspond to the n angles. In this construction, the rotation of the sector blocks can be transformed into translation and symmetry of the system matrix.

The PET detector has n pairs of detection rings. Accordingly, each pixel block conducts n cycles for n angles, and each cycle calculates the system matrix of all LOR corresponding to a certain angle. Every angle corresponds to n LORs, and each pixel block corresponds to the column matrix of $\mathrm{M} = n^2$ elements. Suppose that each sector ring has N_1 pixel blocks, and the first sector ring pixel block is numbered by $1, 2, 3, \cdots N_1$. Then, the corresponding system matrix of each pixel block is:

$$\begin{aligned} A_1 &= [a_{11}, a_{21}, \cdots, a_{i1}, \cdots, a_{M1}]^T \\ A_2 &= [a_{12}, a_{22}, \cdots, a_{i2}, \cdots, a_{M2}]^T \\ &\vdots \qquad\qquad \vdots \\ A_{N_1} &= \left[a_{1N_1}, a_{2N_1}, \cdots, a_{iN_1}, \cdots, a_{MN_1}\right]^T. \end{aligned} \tag{16}$$

Therefore, the system matrix of the whole sector ring is:

$$A = \left[A_1, A_2, \cdots, A_{N_1}\right]. \tag{17}$$

The numbers of pixel blocks in the second sector are $N_1 + 1, N_1 + 2, \cdots, 2N_1 - 1, 2N_1$, which correspond to the first pixel block one by one, so their corresponding system matrix also has a corresponding relationship. In the aforementioned figure, the LORs can be divided into six groups in the circle divided into twelve equal parts. The system matrix of the first group of LOR corresponding to the pixel blocks in the first sector is consistent with the system matrix of the second group of LOR corresponding to the pixel blocks in the second sector. Then, the system matrix values of the corresponding pixel blocks are the same. For example, the system matrix of the pixel blocks numbered t and pixel blocks numbered N_1+t has the following relation:

$$A_{\mathrm{N_1+t,2}} = A_{\mathrm{t,1}}, \tag{18}$$

where A_{ij} is a $(n^2/6) \times 1$ matrix, representing the system matrix of the pixel block corresponding to the jth LOR group of the ith pixel block.

The system matrix corresponding to other LOR groups has the following relationship:

$$\begin{aligned} A_{\mathrm{N_1+t,3}} &= A_{\mathrm{t,2}} \\ A_{\mathrm{N_1+t,4}} &= A_{\mathrm{t,3}} \\ A_{\mathrm{N_1+t,5}} &= A_{\mathrm{t,4}} \\ A_{\mathrm{N_1+t,6}} &= A_{\mathrm{t,5}}. \end{aligned} \tag{19}$$

However, a central symmetry relationship exists in the system matrix of the sixth LOR group corresponding to the pixel blocks in the first sector and the system matrix of the first LOR group corresponding to the pixel blocks in the second sector because their corresponding LOR groups in the same angle are the same, but the arrangement of n LORs at the same angle in the LOR group is opposite. When the entire circular FOV is divided into 12 blocks, and every 30 ° corresponds to the LOR of $n/6$ angles, the above-mentioned central symmetry relationship can be expressed as follows:

$$A_{N_1+t,1,s} = \begin{pmatrix} & & 1 \\ & \iddots & \\ 1 & & \end{pmatrix} \times A_{t,6,s}, \tag{20}$$

where $A_{i,j,s}$ is an $n \times 1$ matrix, representing the system matrix of pixel blocks corresponding to the sth angle LOR of the jth group of the ith pixel block.

$$\begin{pmatrix} & & 1 \\ & \iddots & \\ 1 & & \end{pmatrix} \text{(n ones), denoted as } D_n$$

The system matrix relationship between the sixth group LOR corresponding to the pixel block in the first sector and the first group LOR corresponding to the pixel block in the

second sector can be expressed as follows:

$$A_{N_1+t,1} = \begin{pmatrix} D_n & & & \\ & D_n & & \\ & & \ddots & \\ & & & D_n \end{pmatrix} \times A_{t,6}. \tag{21}$$

The complete system matrix can be fully represented by the system matrix of the corresponding pixel in the first sector. The complete system matrix corresponding to the first sector is denoted as $A_1^{N_1 \times M}$, and the complete system matrix corresponding to the second sector is denoted as $A_2^{N_1 \times M}$. The relationship between the two matrixes is as follows:

$$A_2^{N_1 \times M} = \begin{pmatrix} & & D_n & \\ & & & \ddots \\ & & & D_n \\ 1 & & & \\ & \ddots & & \\ & & 1 & \end{pmatrix} \times A_1^{N_1 \times M}. \tag{22}$$

Based on the above-mentioned LOR rotation invariant property, only a subset of the system matrix is stored (i.e., the relationship between the corresponding LOR of a detector and the adaptive pixel), and the values of the elements of the system matrix that are not stored are obtained by the transformation of the stored subset of the system matrix.

F. ADAPTIVE PIXEL MAPPING

The image is usually stored in the computer in the form of a digital matrix, with the number of pixels in the rows and columns of the matrix equaling the number of pixels in the height and width of the image. However, the matrix and display form of the polar adaptive pixel cannot be the same as that of the conventional image. A mapping function is required to convert it to the traditional square pixel structure.

If the sector ring pixel area weighting method is used to calculate the pixel value, then the weight is considered the ratio of the overlapping area to the total area of the pixel. The calculation is highly complex and irregular. When the square pixel area is smaller than the sector ring pixel area to a certain extent, the square pixel value can be approximately replaced by the sector ring pixel value where the center of the square pixel is located. When the square pixel is subdivided to a certain extent, the image obtained by this method can achieve a high conversion quality. In this method, a function needs to be constructed. The relationship between the square pixels and the sector ring pixels is determined, as shown in the following formula:

$$R_{ij} = \begin{cases} 1 & \text{When square pixel } j \text{ is in the } i \text{ th sector ring} \\ 0 & \text{When square pixel } j \text{ is not in the } i \text{ th fan ring} \end{cases}. \tag{23}$$

Given that the polar adaptive pixel cannot be represented by a multi-row and multi-column matrix like the traditional square pixel, the whole polar adaptive pixel is arranged into a column matrix in the iteration process, where n is the number of pixels. The mapping matrix of the transformation is introduced, and the transformation can be represented by the following formula:

$$I_m = Y_n \times R, \tag{24}$$

where Y_n is the polar coordinate adaptive pixel column matrix, I_m is the square pixel column matrix, and R is the mapping matrix between them. I_m is expressed in the form of a column matrix. Therefore, this matrix needs to be converted into a picture form and rearranged into a 2D matrix.

When the height of the sector ring is h, a square pixel with a side length of $h/2$ is adopted as its mapping target (Fig. 7). The upper and lower sector ring pixels in the right figure are sector ring pixels 1 and 2 in the adaptive pixel, respectively. The center point (orange point) of the four yellow square pixels on the left is located in sector ring pixel 1. Therefore, the mapped value of the yellow square pixel is the pixel value of the sector ring pixel 1, while the center point (dark purple point) of the four purple square pixels on the left is located in the sector ring pixel 2, so the mapped value of the purple square pixel is the pixel value of the sector ring pixel 2.

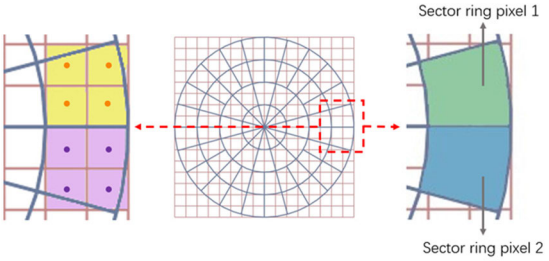

FIGURE 7. Schematic of the mapping.

III. LCLR-PAP ALGORITHM VERIFICATION

A. IMAGE CONVERSION BETWEEN THE POLAR COORDINATES AND THE CARTESIAN COORDINATES

The computer cannot directly output the image formed by the adaptive pixels, so it needs to use the mapping function to convert it into regular square pixels. When the area of the square pixels is smaller than that of the sector ring pixels, the adaptive pixel value at the center of the square pixels can be approximately replaced by the square pixel value. In this section, the pixel resolution in the diameter direction of 200 is taken as the research object to discuss the selection of square pixel resolution. Three concentric ring patterns with the same ring width are selected as the observation objects in the experiment. The square pixel size is nearly the same as the adaptive pixel size (the side length of the square pixel is the same as the adaptive pixel ring height, and the square pixel image resolution is 200 × 200), the square pixel size is about a quarter of the polar coordinate pixel size (the square pixel image resolution is 400 × 400), and the square pixel size is about one-ninth of the polar pixel size (the square pixel image resolution is 600 × 600) for comparison.

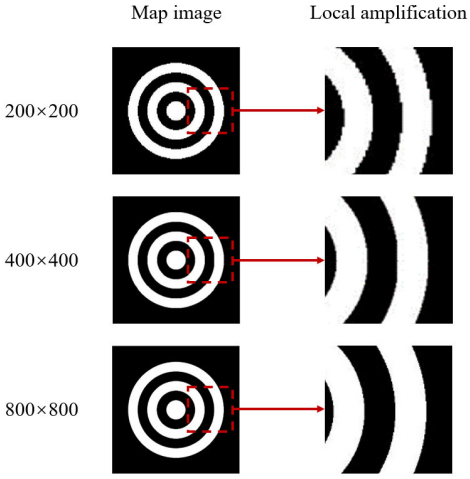

FIGURE 8. Results of the different mapping resolutions.

As shown in Fig. 8, the mapped images of the three resolutions show no change in the image shape after mapping, verifying the correctness of the image mapping conversion. When the resolution of the square pixels is 200 × 200, the image has a jagged shape, low conversion accuracy, and large image quality loss. When the square pixel resolution is 400 × 400, the black and white junction is smooth, and only a few jagged edges can be observed by the naked eye. Accordingly, the image quality is higher, and the conversion accuracy is better. When the square pixel resolution is 600 × 600, the conversion effect is better, but a higher resolution will result in a larger mapping matrix. Significantly increasing the resolution during mapping is unnecessary because the resolution of the reconstructed image itself is low. Therefore, choosing the square pixel as twice the polar adaptive pixel is reasonable.

B. SIMULATION EXPERIMENT RESEARCH

Geant4 is a Monte Carlo application software package developed by CERN, and it is used to simulate the physical process of particle transport in matter. GATE (Geant4 Application for Tomographic Emission) nuclear physics simulation software based on Geant4 can accurately simulate the physical process of positron annihilation by using the Monte Carlo method.

In this section, the simulation data obtained by GATE will be used to compare the image quality of the polar adaptive pixel reconstruction under different image resolutions. The PET detector model in the GATE physical simulation is set according to the Trans-PET system of Suzhou Ruipaining Company, and the main parameters are shown in Table 1.

The Derenzo model is the measured object used in PET simulation (Fig. 9). The diameters of the cylinders in the Derenzo model are 2, 8, 12, and 16 mm from small to large. In the PET simulation experiment, the activity of nuclide injected into the Derenzo cylinder is 800 μ Ci, the detector scanning time is set to 30 s, and the subset of OSEM is 6.

After the simulation experiment, the traditional square pixel system matrix (T-SM) and the compressed polar

TABLE 1. Parameters of Trans-PET.

Parameters	Value
Ring number	48
Crystal number per ring	312
Maximum ring difference	51
Projection angle number	156
LOR number per angle	156
Ring diameter	180 mm
Radial effective FOV	130 mm
Axial effective FOV	100 mm
Crystal size	1.9 × 1.9 × 10 mm3
Crystal spacing	2.0 × 2.0 mm2
Time resolution	1.5 ns
Spatial resolution	0.99 mm
Average energy resolution	15%
Energy window	350–625 KeV

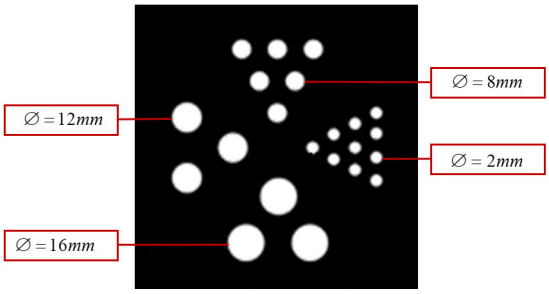

FIGURE 9. Derenzo model.

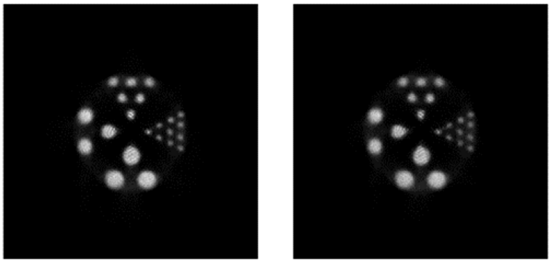

(a) Adaptive pixel reconstruction (b)Traditional method reconstruction

FIGURE 10. Reconstruction effects of two system matrices.

adaptive pixel system matrix (PAP-SM) are used for reconstruction, and the 29th slice of the Derenzo model is selected for a comparative study. According to the result of the comparison of the images reconstructed with the T-SM and those reconstructed with the compressed PAP-SM, the latter can achieve the same effect (Fig. 10). In the 400 × 400 image reconstruction, the system matrix is compressed by nearly 14.9 times.

We draw the gray value of the pixel wherein the red line passes through in the reconstructed image into a sectional curve to compare the difference between the slices of the two kinds of system matrix reconstruction, as shown in Fig. 11. The reconstruction effect of the PAP-SM reconstruction is

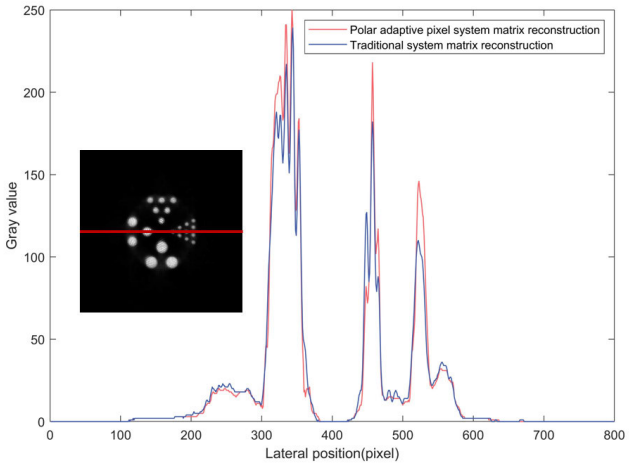

FIGURE 11. Section line position and two kinds of system matrix reconstruction section diagram.

similar to that of the complete T-SM reconstruction, and the overall change trend is the same. The image reconstructed by the PAP-SM has a good performance on peak value, indicating that the system matrix has no loss after compression by this algorithm, and such pixel division is feasible for reconstruction.

Based on the result of the reconstruction time of the two system matrices, compared with the T-SM, the reconstruction time required by the PAP-SM is reduced by about 24.8%, as shown in Fig. 12. This phenomenon occurs because after the detection field is set to circular, compared with the square detection field, only fewer pixels can be seen in four corners. Accordingly, the total number of pixels and the number of pixels needed to iterate are less. Therefore, the iteration time is shorter, indicating that the algorithm can not only compress the system matrix but also reduce the iteration time in the reconstruction process.

The curves of the number of iterations and the signal-to-noise ratio (SNR) of the two forms of system matrix reconstruction are calculated and drawn to verify the convergence of the algorithm, as shown in Fig. 13. The aforementioned figure demonstrates that the curve changes of the two forms of system matrix are similar. The SNR rapidly rises during one to five iterations and then tends to be flat. After 20 iterations, the SNR tends to a relatively fixed value. The result of the comparison of the two curves indicated that the SNR of the system matrix constructed by using PAP-SM is better than that of the traditional system matrix. The SNR of 20-40 iterations of the two system matrices is shown in Table 2, and the average SNR improvement rate is about 4.35%. The possible reason is that the number of iterative pixels is reduced, so the impact of some noises in the simulation process is minimized, demonstrating that the algorithm is feasible in image reconstruction.

Theoretically, the higher the resolution of the reconstructed image, the clearer the details. However, the experiment indicated that the higher the resolution of the reconstructed image

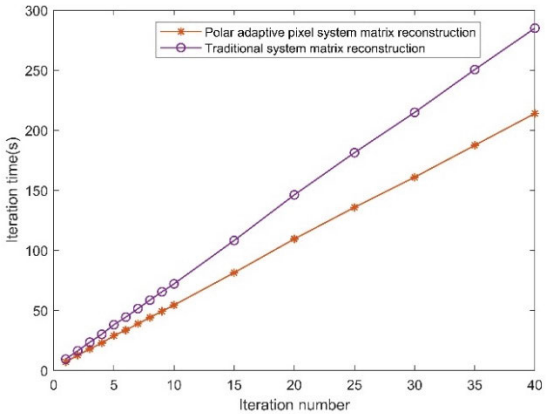

FIGURE 12. Comparison of the reconstruction time between the two matrix systems.

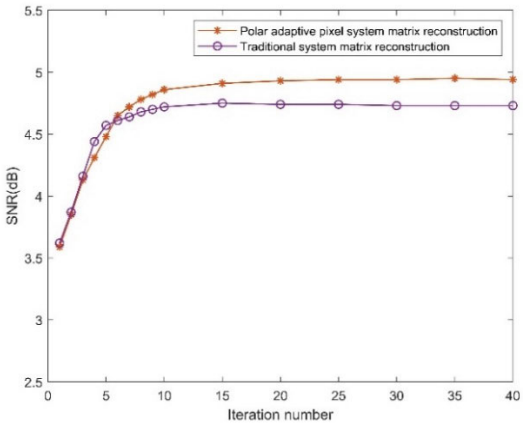

FIGURE 13. Comparison of the reconstruction SNR between the two matrix systems.

is not the better. The slice images of 200 × 200, 400 × 400, and 800 × 800 sizes are reconstructed using the PAP-SM, and the reconstructed image effects under three kinds of reconstructed image resolutions are compared.

From the reconstructed image shown in Figure 13, it can be seen that when the size of the reconstructed image is 200 × 200, all four diameters of cylinders produce large distortion, and the cylinders with 2 mm diameter have different sizes and are difficult to distinguish. When the size of the reconstructed image is 400 × 400, the overall shape of the cylinder is neat, no obvious deformation occurred, and the spacing between the cylinders is clear and can be distinguished. In particular, the overall shape of the cylinder with a 2 mm diameter is clear, and the reconstruction result is better than that of 200 × 200. However, when the size of the reconstructed image is 800 × 800, the 2 mm diameter cylinders become somewhat blurred, and the image as a whole is not clearer. Therefore, we use 400 × 400 reconstructed images for algorithm analysis.

C. OPTIMIZATION RESULTS

In the process of pixel adaptive division, this paper optimizes the size difference of pixel area in the central position of the image. As shown in the left figure of Fig. 15, if not optimized,

TABLE 2. SNR of reconstruction.

Iteration number	20	25	30	35	40
SNR(T-SM)	4.93	4.94	4.94	4.95	4.94
SNR(PAP-SM)	4.74	4.74	4.73	4.73	4.73
improvement rate	4.01%	4.22%	4.44%	4.47%	4.44%
Average improvement rate			4.35%		

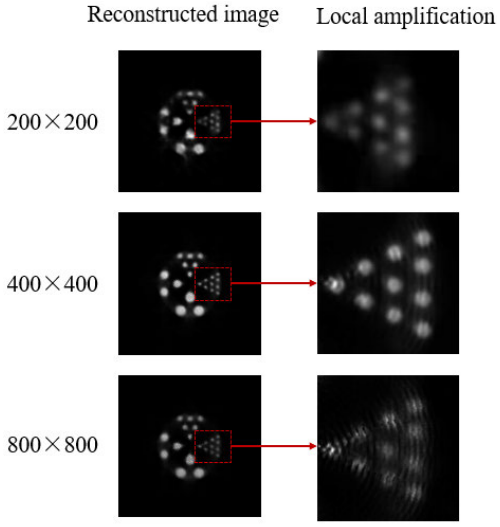

FIGURE 14. Image reconstructed by the adaptive system matrix under three resolutions.

black shadows will be caused due to the non-uniformity of pixel size, resulting in a loss of image quality.

The system matrix calculation and image reconstruction are reperformed again according to the above-mentioned method. The other settings are consistent with the simulation settings of the Derenzo model except for the system matrix. The 29th slice after the simulation is selected, as shown in Fig. 15. The shadow at the center of the reconstructed image is improved.

We plot the grayscale values of the pixels passing through the red line in the reconstructed image as the profile curve to further compare the differences between the reconstructed slice maps before and after the optimization, as shown in Fig. 16. The trend of the curve also shows that the closer to the center, the area difference before the optimization is larger and the pixel black shadow is more serious. Meanwhile, the structural similarity (SSIM) is calculated for the reconstructed images before and after optimization, and the results are shown in Table **3**. The optimized PAP-SM solved the black shadows problem and improved the structural similarity of the reconstructed images in the reconstruction process.

D. DISCUSSION

This paper is proposed to address the system matrix of γ-photon in industrial nondestructive testing applications facing too large. After calculation, it can be found that the

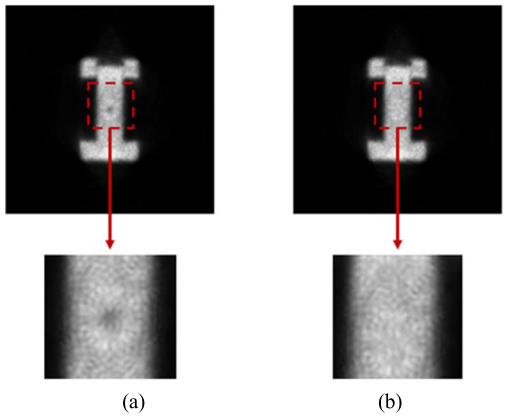

FIGURE 15. Reconstructed images: (a) before optimization and (b) after optimization.

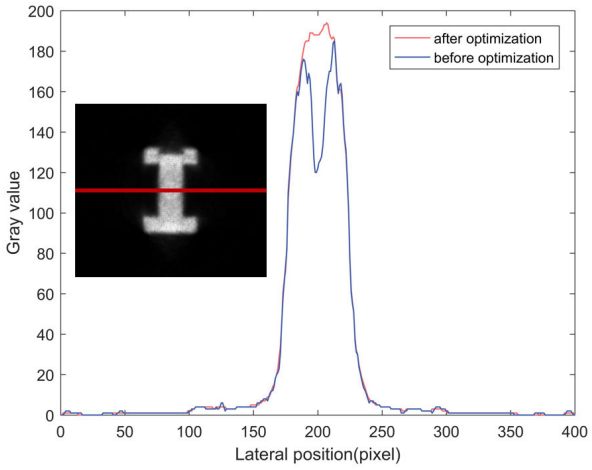

FIGURE 16. Section line position and reconstruction section diagram before and after optimization.

circular slice is divided into N parts by using the optimized segmentation PAP algorithm, considering only geometric symmetry. The division depends on the structure of the PET detector. In this paper according to the PET detector used in the experiment set N to 12, the system matrix can be compressed to the original 1/ 14.9, and the calculation time of the high-precision system matrix can be shortened to 1/14.9 of the original one. Taking the two-dimensional reconstruction as an example, when the number of coincidence events is 156×156 and the size of the reconstructed image is 400×400, the size of the system matrix is 14.51GB, which can be compressed to 4.13MB by combining with the sparsity of the matrix, achieving a data compression of 3513.3 times; Taking three-dimensional reconstruction as an example when the number of coincidence events is $156\times156\times52\times52$ and the size of the reconstructed image is $400\times400\times52$, the size of the system matrix is 1.95PB. Combined with the sparsity and axial compression of the matrix, the size of the system matrix can be compressed to 6.94GB, which is enough to import all into memory (video memory) for subsequent iterative calculations. While compressing the system matrix, this paper

TABLE 3. SSIM of reconstruction.

	SSIM (iteration number: 20)	SSIM (iteration number: 25)	SSIM (iteration number: 30)
After optimization	0.8338	0.8351	0.8346
Before optimization	0.8225	0.8240	0.8234
increase rate	1.37%	1.35%	1.36%
Average improvement rate		1.36%	

proposes a linear recovery algorithm of the system matrix for the special characteristics of the PAP pixel division, using the LOR rotation invariance and the rotational overlap of the detector to represent the recovery of the system matrix by a matrix multiplication, which solves the complexity of the existing system matrix recovery algorithm.

In the study, the system matrix after PAP division (PAP-SM) is reconstructed by iterative method with the traditional system matrix (T-SM), which is the most widely used iterative reconstruction algorithm at the present stage, and their iteration times and SNRs of reconstructed images are compared. The SNR of the reconstructed image of the PAP-SM iteration and T-SM both tend to a fixed value after 15-20 iterations, and the fixed value of PAP-SM is slightly improved compared with the fixed value of T-SM. In the case of the same number of iterations, the reconstruction time of PAP-SM is shorter, so PAP-SM is feasible in image reconstruction.

Meanwhile, for the PAP reconstruction algorithm, this paper selects the resolution of the reconstructed image. When the reconstructed image size is 400×400, compared with the reconstructed images of 200×200 and 800×800, the image reconstruction effect is better. There is no obvious deformation in the vision, and the interval is clear and distinguishable. Therefore, the reconstruction resolution of 400×400 and the corresponding system matrix model are used in this paper. Aiming at the case of uneven center pixels of the image, the optimization algorithm of uniform pixels in the center position is adopted. By comparing the center section line and structural similarity with the reconstructed image before optimization, the pixel value step (plunge) of the section line graph is improved, the overall structural similarity of the image is increased, and the optimized reconstructed image can truly reflect the nuclide information at the center of the image.

IV. CONCLUSION

In this work, a new method is proposed to fully utilize the rotational invariance of the LOR and the rotation of the detector FOV to address the following issues: the large detection range and high resolution of the γ-photon tomography system; the high-quality system matrix occupies a substantial amount of storage space; the high precision system matrix generation takes a long time; and the existing compression methods of pixel partition or system matrix recovery is complicated. The system matrix of the entire FOV can be obtained by calculating the system matrix from a sector area in the FOV. This method not only compressed the system matrix but also greatly reduced the amount of calculation in the process of establishing the system matrix. Under the design of polar coordinates and adaptive system matrix, this rotation will not bring position deviation and pixel edge cutting. The compression of the system matrix is lossless and the recovery is quick and direct. Experiments on the compressed polar adaptive pixel system matrix (PAP-SM) verify the correctness of the lossless recovery of the system matrix and the effectiveness of the reconstruction, and the reconstruction speed and image quality are also improved compared with the image reconstruction of the traditional system matrix (T-SM). For the problem of black shadows caused by uneven pixel size in the center of the reconstructed image, the pixel division in this part is optimized, and the image quality is significantly improved after the optimization. Therefore, the proposed algorithm can provide an efficient scheme for solving the large-scale system matrix compression-recovery, and a feasible scheme for the application of γ-photon industrial nondestructive testing and in-situ detection, which is conducive to expanding the application of γ-photon tomography technology in the industry, and makes it possible to apply the technology in high-resolution industrial nondestructive testing.

REFERENCES

[1] S. S. Obaid, M. I. Sayyed, D. K. Gaikwad, and P. P. Pawar, "Attenuation coefficients and exposure buildup factor of some rocks for gamma ray shielding applications," *Radiat. Phys. Chem.*, vol. 148, pp. 86–94, Jul. 2018, doi: 10.1016/j.radphyschem.2018.02.026.

[2] M. Yao, Y. Zhang, M. Zhao, R. Guo, and J. Xu, "Research on combustion flow field imaging method based on ray casting algorithm," *AIP Adv.*, vol. 9, no. 5, pp. 055022-1–055022-11, May 2019, doi: 10.1063/1.5042043.

[3] K. S. Alzimami, S. A. Sassi, and N. M. Spyrou, "A comparison between 3D OSEM and FBP image reconstruction algorithms in SPECT," in *Proc. DBLP*, vol. 39, Jan. 2009, pp. 195–206, doi: 10.1007/978-90-481-2311-7_17.

[4] K. Lange and R. Carson, "EM reconstruction algorithms for emission and transmission tomography," *J. Comput. Assist. Tomogr.*, vol. 8, no. 2, pp. 306–316, Apr. 1984.

[5] M. J. Roef, S. Rijnsdorp, C. Brouwer, D. N. Wyndaele, and A. J. Arends, "Evaluation of quantitative ga-68 PSMA PET/CT repeatability of recurrent prostate cancer lesions using both OSEM and Bayesian penalized likelihood reconstruction algorithms," *Diagnostics*, vol. 11, no. 6, p. 1100, Jun. 2021, doi: 10.3390/diagnostics11061100.

[6] V. Y. Panin, F. Kehren, H. Rothfuss, D. Hu, C. Michel, and M. E. Casey, "PET reconstruction with system matrix derived from point source measurements," *IEEE Trans. Nucl. Sci.*, vol. 53, no. 1, pp. 152–159, Feb. 2006, doi: 10.1109/TNS.2005.862979.

[7] M. Rafecas, G. Boning, B. J. Pichler, E. Lorenz, M. Schwaiger, and S. I. Ziegler, "Effect of noise in the probability matrix used for statistical reconstruction of PET data," *IEEE Trans. Nucl. Sci.*, vol. 51, no. 1, pp. 149–156, Feb. 2004, doi: 10.1109/TNS.2003.822998.

[8] C. Hao, M. Zhao, M. Yao, R. Guo, M. Zhu, and X. Hui, "Positron emission tomography of not-full-ring sensors arrangement: Simulation and verification for internal imaging of hydraulic cylinder," *IEEE Access*, vol. 8, pp. 208096–208106, 2020, doi: 10.1109/ACCESS.2020.3038661.

[9] S. Ibrahim, M. A. M. Yunus, R. G. Green, and K. Dutton, "Concentration measurements of bubbles in a water column using an optical tomography system," *ISA Trans.*, vol. 51, no. 6, pp. 821–826, Nov. 2012, doi: 10.1016/j.isatra.2012.04.010.
[10] Z. Z. Deng, S. K. Xu, Z. Chen, K. Zhou, and W. Y. Hong, "Research on system response matrix modelling method of rectangular PET scanner based on Monte Carlo simulation," *J. Instrum.*, vol. 16, no. 1, Jan. 2021, Art. no. P01009, doi: 10.1088/1748-0221/16/01/P01009.
[11] D. J. Kadrmas, "Rotate-and-slant projector for fast LOR-based fully-3-D iterative PET reconstruction," *IEEE Trans. Med. Imag.*, vol. 27, no. 8, pp. 1071–1083, Aug. 2008, doi: 10.1109/TMI.2008.918328.
[12] B. Zhang, B. Shan, M. Yun, and S. Zhao, "A complete implementation of list-mode reconstruction for PET," *Nucl. Sci. Techn.*, vol. 23, no. 4, pp. 219–225, Aug. 2012, doi: 10.13538/j.1001-8042/nst.23.219-225.
[13] R. L. Siddon, "Fast calculation of the exact radiological path for a three-dimensional CT array," *Med. Phys.*, vol. 12, no. 2, pp. 252–255, Mar./Apr. 1985, doi: 10.1118/1.595715.
[14] J. Qi, R. M. Leahy, S. R. Cherry, A. Chatziioannou, and T. H. Farquhar, "High-resolution 3D Bayesian image reconstruction using the microPET small-animal scanner," *Phys. Med. Biol.*, vol. 43, no. 4, pp. 1001–1013, Apr. 1998, doi: 10.1088/0031-9155/43/4/027.
[15] J. Zhou and J. Qi, "Fast and efficient fully 3D PET image reconstruction using sparse system matrix factorization with GPU acceleration," *Phys. Med. Biol.*, vol. 56, no. 20, pp. 6739–6757, Oct. 2011, doi: 10.1088/0031-9155/56/20/015.
[16] F. Meng, J. Cheng, C. Li, Y. Shi, G. Zhang, X. Lyu, W. Qin, and S. Zhu, "Model construction of photon propagation based on the geometrical symmetries and GPU technology for the quad-head PET system," *J. Instrum.*, vol. 15, no. 12, Dec. 2020, Art. no. P12015, doi: 10.1088/1748-0221/15/12/P12015.
[17] M. Rafecas, "Use of a Monte–Carlo based probability matrix for 3D iterative reconstruction of MADPET-II data," in *Proc. Nucl. Sci. Symp. Conf. Rec.*, Portland, OR, USA, 2003, pp. 1775–1779.
[18] F. R. Rannou and A. F. Chatziioannou, "Fully 3D system model estimation of OPET by Monte Carlo simulation," in *Nucl. Sci. Symp. Conf. Rec.*, Rome, Italy, 2004, pp. 3433–3436.
[19] J. J. Scheins, H. Herzog, and N. J. Shah, "Fully-3D PET image reconstruction using scanner-independent, adaptive projection data and highly rotation-symmetric voxel assemblies," *IEEE Trans. Med. Imag.*, vol. 30, no. 3, pp. 879–892, Mar. 2011, doi: 10.1109/TMI.2011.2109732.
[20] Y. H. Yu, Y. Xia, J. Chen, B. Hong, Y. Liu, S. Wang, and T. Y. Ma, "PET image reconstruction with rotationally symmetric polygonal pixel grid based highly compressible system matrix," *Nucl. Sci. Tech.*, vol. 3, pp. 6–17, Jan. 2013.
[21] A. M. Ahmed, Y. Kikuchi, S. Matsuyama, A. Terakawa, S. Takyu, H. Sugai, and K. Ishii, "Pre-computed system matrix calculation based on a piecewise method for PET," *Radiol. Phys. Technol.*, vol. 8, no. 1, pp. 88–96, Jan. 2015, doi: 10.1007/s12194-014-0293-y.
[22] X. Sun, Y. Li, L. Yang, S. Wang, B. Zhang, P. Xiao, and Q. Xie, "Fast and accurate Monte-Carlo based system response modeling for a digital whole-body PET," in *Conf. Phys. Med. Imag., Orlando, FL, USA*, vol. 2017, p. 101321H.
[23] L. Kaufman, S. Morgenthaler, and Y. Vardi, "Maximum likelihood reconstruction in emission tomography with time of flight information: A limited," Massachusetts Inst. Technol., Cambridge, MA, USA, Tech. Rep. TR-ONR-33, Sep. 1983.
[24] H. M. Hudson and R. S. Larkin, "Accelerated image reconstruction using ordered subsets of projection data," *IEEE Trans. Med. Imag.*, vol. 13, no. 4, pp. 601–609, Dec. 1994, doi: 10.1109/42.363108.
[25] S. Shiba and H. Sagara, "Passive gamma emission tomography with ordered subset expectation maximization method," *Ann. Nucl. Energy*, vol. 150, Jan. 2021, Art. no. 107823, doi: 10.1016/j.anucene.2020.107823.
[26] Y. Xin, M. Pawlak, and S. Liao, "Accurate computation of Zernike moments in polar coordinates," *IEEE Trans. Image Process.*, vol. 16, no. 2, pp. 581–587, Feb. 2007, doi: 10.1109/TIP.2006.888346.

SHUYI CHEN was born in Sanming, Fujian, China, in 1999. She received the B.Sc. degree from the Nanjing University of Aeronautics and Astronautics, China, in 2021, where she is currently pursuing the master's degree with the School of Automation. Her research interests include positron nondestructive testing, image processing, and algorithm optimization.

MIN ZHAO is currently a Professor and a Ph.D. Supervisor with the Nanjing University of Aeronautics and Astronautics. His current interests include UAV trajectory planning and control, positron annihilation technology for nondestructive testing, computer measurement, and control system for high-speed railway nondestructive testing. He is a member of the Metrology Technology Professional Committee, Chinese Society of Aeronautics and Astronautics, the Vice Chairperson of the Thermal Engineering Professional Committee, Jiangsu Institute of Metrology and Testing, and the Chairperson of the Supervisory Board, Jiangsu Institute of Instrumentation.

MIN YAO received the B.Sc., M.Sc., and Ph.D. degrees from the Nanjing University of Aeronautics and Astronautics, China, in 1997, 2002, and 2008, respectively. She is currently an Associate Professor with the Nanjing University of Aeronautics and Astronautics. Her research interests include computer measurement, control and UAVs task assignment, data and signal processing, and algorithm optimization.

RUIPENG GUO received the Ph.D. degree in instrument science and technology from Shanghai Jiao Tong University, Shanghai, China, in 2011. She is currently an Associate Professor with the Nanjing University of Aeronautics and Astronautics. Her research interests include nondestructive testing, computer measurement, and control and signal processing.

MING WANG received the M.Sc. degree from the Harbin University of Science and Technology, in 2020. He is currently pursuing the Ph.D. degree with the Nanjing University of Aeronautics and Astronautics. His main research interests include positron nondestructive testing, algorithm optimization, and 3D image reconstruction algorithms based on AI.